Computational applications of the many-interacting-worlds interpretation of quantum mechanics

Simone Sturniolo*

Scientific Computing Department, STFC, Rutherford Appleton Laboratory, Harwell Campus, Didcot OX11 0QX, United Kingdom

While historically many quantum-mechanical simulations of molecular dynamics have relied on the Born-Oppenheimer approximation to separate electronic and nuclear behavior, recently a great deal of interest has arisen in quantum effects in nuclear dynamics as well. Due to the computational difficulty of solving the Schrödinger equation in full, these effects are often treated with approximate methods. In this paper, we present an algorithm to tackle these problems using an extension to the many-interacting-worlds approach to quantum mechanics. This technique uses a kernel function to rebuild the probability density, and therefore, in contrast with the approximation presented in the original paper, it can be naturally extended to n-dimensional systems. This opens up the possibility of performing quantum ground-state searches with steepest-descent methods, and it could potentially lead to real-time quantum molecular-dynamics simulations. The behavior of the algorithm is studied in different potentials and numbers of dimensions and compared both to the original approach and to exact Schrödinger equation solutions whenever possible.

I. INTRODUCTION

Since its introduction [1], *ab initio* molecular dynamics has been widely used to study a range of different systems. Historically, these simulations have always relied on the Born-Oppenheimer approximation [2] to separate electronic and nuclear motions, treating the first with quantum mechanics and the latter with classical Newtonian mechanics. In recent years, however, interest has arisen in the relevance of quantum effects in nuclear motions, as advances in computational technology have made their calculation more practical. Many calculations and experiments show that nuclear quantum effects, especially involving the motion of hydrogen nuclei, are relevant to fully describe the behavior of water and ice [3,4] in strongly hydrogen-bonded systems [5] and in biological macromolecules [6]. Simulating these effects is no easy feat. One of the most popular approaches is that of path-integral molecular dynamics (PIMD) [7], which allows one to approximate quantum statistical distributions by replacing a single nucleus with many copies of it organized as beads in a closed loop, all behaving classically except for a fictitious harmonic potential term linking them together. Since the dynamics of a system defined in this way is not necessarily physical anymore, different conventions can be adopted for the effective masses of its various vibrational modes depending on the quantities of interest [8], such as centroid molecular dynamics (CMD) [9], ring polymer molecular dynamics (RPMD) [10], and the one that is most commonly referred to as PIMD proper. This technique has been used successfully to explore problems such as the behavior of hydrogen atoms shared by molecules in water monolayers on metal surfaces [3], the quantum nature of the hydrogen bond [11], and bimolecular reaction rates [12], using both *ab initio* methods and parametrized potentials. Hall,

Deckert, and Wiseman proposed a possible interpretation of quantum mechanics that shares many features with PIMD [13]. In that approach, which the authors called many interacting worlds (MIW), quantum-mechanical behavior emerges from many copies of the same particle all interacting with each other through a potential that has no classical equivalent. As opposed to PIMD, however, this potential is repulsive, which means MIW could describe a quantum ground state as an equilibrium configuration; in addition, MIW is theoretically an approximation to full quantum dynamics, meaning it should be able to simulate time-dependent quantum evolution. This makes it a promising avenue to explore for the development of new computational techniques for the treatment of nuclear quantum effects. However, while the theory presented in [13] is general, the practical implementation proposed in the paper can be applied only to one-dimensional systems. In this paper, we develop a different approach that is naturally extensible to higher dimensions and could therefore be put to practical use in molecular-dynamics simulations.

II. THE MANY-INTERACTING-WORLDS APPROACH

A. Theory

The MIW approach, as presented in [13], can be considered as a discretization of the Holland-Poirier hydrodynamical approach to QM [14,15] or it can be derived from the well-known de Broglie–Bohm pilot wave interpretation [16,17]. For the full derivation, we direct the reader to the original paper. Here we just give an outline of the fundamentals of this approach. The system to be described is represented by a number of worlds N, with a multiworld configuration at time t,

$$\mathbf{X}(t) = \{\mathbf{x}_1(t), \mathbf{x}_2(t), \ldots, \mathbf{x}_N(t)\} \qquad (1)$$

with every $\mathbf{x}_n(t) = [x_{1,n}(t), x_{2,n}(t), \ldots, x_{K,n}(t)]$ being the total classical configuration of world n, namely an array of the K degrees of freedom of the system. For a generic D-dimensional

*simone.sturniolo@stfc.ac.uk

system containing Q particles, it will be $K = QD$. It is easy to see then how the probability density to find the system in a configuration $\mathbf{q}$, equivalent to the square modulus of the wave function in the usual Schrödinger's picture, can be approximated as

$$P(\mathbf{q},t) = |\Psi(\mathbf{q},t)|^2 \sim \sum_{n=1}^{N} \delta(\mathbf{q} - \mathbf{x}_n(t)) \qquad (2)$$

using the Dirac δ distribution. The dynamics of the system are governed by the usual laws of Newtonian mechanics. The classical Hamiltonian can be written as

$$\mathbb{H}_{\mathrm{MIW}}(\mathbf{X}) = \sum_{n=1}^{N} \left[\sum_{k=1}^{K} \frac{1}{2} m_k \dot{x}_{k,n}^2 + V(\mathbf{x}_n) \right] + U_{\mathrm{MW}}(\mathbf{X}), \quad (3)$$

where the quantities with index k (masses, coordinates, etc.) correspond to each individual particle, and the potential is a function of the entire world's configuration. One can distinguish a term that operates on each world configuration separately (with the classical potential V also including any regular interactions among particles, like electrostatic forces) and an interworld potential U_{MW}, which is nonclassical in nature and introduces quantum effects. For example, delocalization is the consequence of U_{MW} being repulsive and preventing all particles from finding an equilibrium in the potential minimum, and energy indeterminacy is the consequence of energy being exchanged between worlds thanks to the interworld coupling and therefore not being conserved in each separate world (while the overall many-world ensemble is indeed conservative). The general form of U_{MW} is

$$U_{\mathrm{MW}}(\mathbf{X}) = \sum_{n=1}^{N} \sum_{k=1}^{K} \frac{1}{2m_k} \left[g_N^k(\mathbf{x}_n; \mathbf{X}) \right]^2, \qquad (4)$$

where

$$g_N^k(\mathbf{q}; \mathbf{X}) \approx \frac{\hbar}{2} \frac{1}{P(\mathbf{q}; \mathbf{X})} \frac{\partial P(\mathbf{q}; \mathbf{X})}{\partial q_k}. \qquad (5)$$

Here P represents the distribution describing the probability of finding the system in a given configuration $\mathbf{q}$, as in Eq. (2), but its dependence from the configuration of the "world particle" $\mathbf{X}$ is made explicit. From Eqs. (4) and (5) it is clear that to run a simulation based on the MIW approach, it is necessary to rebuild the probability density function $P(\mathbf{q}; \mathbf{X})$ in some approximated way for a given multiworld configuration. This is implied in the choice of only writing an "approximate" equality in Eq. (5). Equation (2) suggests one way to do this, but it is obvious that in practical computation, where limits on available power and time will force one to use a small number of worlds N, this method would fail rather badly. In [13], the authors propose for the 1D case of a single particle an approximation

$$P(x_n) \approx \frac{1}{N(x_{n+1} - x_n)}. \qquad (6)$$

Here x_n has become a scalar, since each world has only one degree of freedom. This equation holds whenever the distance between the same particle in adjacent worlds is slowly varying and by enforcing that $x_{n+1} > x_n$ all the time, and it does indeed produce good results. This leads to an interworld potential depending overall on five worlds—the world of interest n and its first and second neighbors. It has,

however, two problems that prevent it from being applicable to general purpose simulations, namely that it cannot be naturally extended to more than one dimension and that it features a divergent potential that makes numerical integration very sensitive to the time step used when any two world particles happen to be close enough. In this paper, we suggest a different method to compute the probability density, which overcomes these problems using the technique known as kernel density estimation (KDE) [18,19]. The idea is simply to apply a kernel distribution $\mathcal{K}$ to Eq. (2), so that

$$P(\mathbf{q}) = \sum_{n=1}^{N} \mathcal{K}(\mathbf{q} - \mathbf{x}_n). \qquad (7)$$

In this way, and with a good choice of function $\mathcal{K}$, $P(\mathbf{q})$ is continuous and differentiable on all space, which leads to a natural way of computing the quantum forces, and can be defined similarly for any dimensionality. A very similar approach has been proposed in parallel to this work by Herrmann and the authors of the original MIW paper in [20]. In that, a more natural multidimensional extension of the original method by using Delaunay triangulations is explored as well, but it is found to be inconvenient for practical applications due to the discontinuities it introduces in the dynamics. When using KDE, an obvious choice is to make the kernel function Gaussian, which, including the necessary normalization conditions, returns:

$$P(\mathbf{q}) = \frac{1}{N(\sqrt{\pi}b)^D} \sum_{n=1}^{N} \exp\left[-\frac{(\mathbf{q} - \mathbf{x}_n)^2}{b^2} \right] \qquad (8)$$

with b a free kernel bandwidth parameter and D the number of dimensions of the system. It is then possible to derive analytically the potential and the forces. While the process is not especially complex, the calculations are long, and they are reported in Appendix A. The Gaussian kernel, however, has the potential to give rise to a problem. Let us consider the case of a simulation of a single quantum particle. From now on, it must be clear that when we talk about "particles" we mean in fact multiple classical copies of the same particle across worlds interacting only through the interworld potential, and not effectively different particles interacting classically. Due to the appearance of the derivative of P in Eq. (5), one can see after deriving the forces that it will give rise to no repulsion when two particles are close enough or overlapping. This runs counter to physical intuition: since the interworld potential must reproduce the effects of what we could call "quantumness" on the system, it should be generally repulsive to avoid the wave function collapsing in a single spot and losing position indeterminacy. This is a property of any symmetric and smooth kernel, as its derivative in the center will always be null. Therefore, if the particles happened to get closer than a certain distance during the simulation, they might end up coalescing, and this artifact would compromise the final result. For this reason, we test also a different kernel, with a discontinuous, nonzero derivative in the origin:

$$P(\mathbf{q}) = \frac{\Gamma(D/2)}{2N(D-1)!(\sqrt{\pi}b)^D} \sum_{n=1}^{N} \exp\left[-\frac{|\mathbf{q} - \mathbf{x}_n|}{b} \right], \quad (9)$$
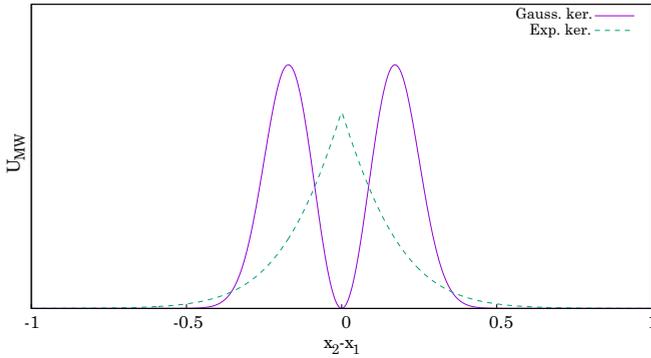
FIG. 1. Many-world potential for $N = 2$ and for the cases of Gaussian and exponential kernels. It can be seen how the former features a minimum for the case of overlapping particles where the latter has a cusp. Units are arbitrary.

where the proper normalization factor has been inserted in front (with Γ denoting the Gamma function). Since this factor is less obvious, proof of how it is derived is provided in Appendix B. Figure 1 compares the U_{MW} for two particles as the distance between them varies for both kernels and highlights the problem and the way the exponential kernel solves it. Potential and forces can be found for this kernel similarly to what has been seen with the Gaussian one, and they are written out in Appendix A as well.

In Sec. III we will proceed to test the MIW method in some numerical simulations on toy models and compare its results with both solutions obtained by traditional methods based on diagonalization of the Hamiltonian and, for the case of 1D problems, MIW simulations carried out with the potential derived from Eq. (6).

B. Comparison with methods of the PIMD family

Given the similarities between the two techniques, it is worth the effort to explore a bit more the analogies and differences between MIW and PIMD-like methods (PIMD, CMD, and RPMD) to better evaluate the potential applicability of this approach. From now on, I will refer to all these latter three methods as PIMD unless specified otherwise. As mentioned already, MIW and PIMD share a fundamental similarity in their approach to simulating quantum effect, as both use a number of classical simulations coupled by a fictitious potential to reproduce quantum statistics. The potential that couples PIMD beads, however, is harmonic and works only between next-neighbor worlds, which in turn allows us to treat the dynamics by separating independent harmonic modes. This is not possible in kernel MIW, where the potential is strongly nonlinear and couples all worlds with all others. Nevertheless, the formal similarities mean that for a lot of existing software packages implementing MIW dynamics could probably be a relatively easy task, as it could reuse much of the PIMD code. With regard to performance, these two methods tend to be complementary, and that makes it hard to set up a direct comparison. A key feature of PIMD methods is that the number of beads required to converge a calculation increases dramatically as the temperature approaches 0 K [21]. Therefore, PIMD methods tend to perform better at higher temperatures. Conversely, the

theory behind MIW simulations justifies best their use for searching the ground state, and therefore the low-temperature limit. In addition, the harmonic potential featured in PIMD is attractive; the equilibrium configuration for the beads would be one where they all sit in the same potential minimum, and therefore the dynamical simulation is vital to actually sample quantum statistics. The MIW potential, on the other hand, is repulsive, and its equilibrium should correspond to an approximation of the quantum ground state. This means that it should be possible to find ground-state densities using not only molecular dynamics, but even common optimization algorithms such as BFGS [22]. While, as seen in the next section, MIW calculations seem to require slightly higher numbers of worlds than a typical room-temperature PIMD simulation (for which 16 or 32 beads are common values), the increased calculation load can be amply compensated by replacing a costly and long molecular-dynamics simulation with a simple geometry optimization. This strategy is explored in the next section. Finally, there's the issue of real-time quantum dynamics. While PIMD technically computes an evolution in imaginary time, and thus cannot be directly interpreted as a dynamical process, it is possible with both CMD and RPMD to compute quantum time correlation functions [8,23]. Ideally, MIW simulations should be able to achieve a similar result in a more immediate way, as they represent evolution in real time instead. However, the accuracy of this evolution is limited by how well the quality of the reconstructed density is preserved, and errors accumulating through time will probably cause time correlation functions to be accurate only on a short time scale.

III. SIMULATION DETAILS

Numerical simulations were carried out on a personal computer using PYTHON and the scientific libraries Numpy and Scipy for matrix diagonalizations and optimization operations [24,25].

When necessary, the exact solution results in 1D were obtained by building a Hamiltonian based on a matrix Numerov method [26]. This approach was then expanded to higher dimensionality; the details are explained in Appendix C. Since this method uses a direct space basis set, all potentials are treated effectively as if they were enclosed in an infinite well. Whenever harmonic potentials appear, the known analytical solutions for ground-state energies and wave functions are used. For the MIW method, the equations of motion were integrated using a standard velocity Verlet algorithm, and a Langevin thermostat was used for thermalization when required. In addition, an adaptive time step has been used, where at any given step i,

$$dt_i = \min\left(dt_0 \frac{\max(|F_0|)}{\max(|F_i|)}, dt_{\max}\right), \tag{10}$$

so that dt scales with the maximum force present in the system. Particular attention, of course, must be paid to the initial estimate of the bandwidth parameter, b, which controls the radius of the interaction. This is a common problem in kernel density estimation, well known in statistics. Given the particle positions, one has to find the kernel width that best fits the target probability distribution. For cases in which the initial desired probability distribution is known (for example, when

initializing a simulation with knowledge of the ground state), the AMISE method was used. For those where instead only an educated guess was possible, the Silverman method was employed. Both of these methods are described in [27].

IV. RESULTS

A. Energy

In these tests, we focus on the performance of the MIW approach in dealing with the ground state of a proton in a few example potentials. We initialize the MIW system by using the known ground-state probability density obtained from diagonalizing the Hamiltonian, and we consider the error in the energy so obtained in order to compare the different kernels and dimensionalities in ideal conditions. The potentials used are of two types. One is a simple harmonic potential of the form

$$V_{\text{harm}}(\mathbf{x}) = \frac{k}{2}\mathbf{x}^2 \qquad (11)$$

while the other is a multidimensional Lennard-Jones potential with an angular term of the form

$$V_{lj}(\mathbf{x}) = \Delta V_r\left[\left(\frac{|\mathbf{x} - \mathbf{x}_0|}{r_0}\right)^{-12} - 2\left(\frac{|\mathbf{x} - \mathbf{x}_0|}{r_0}\right)^{-6}\right]$$
$$+ \Delta V_\alpha\left(1 - \frac{\mathbf{x} - \mathbf{x}_0}{|\mathbf{x} - \mathbf{x}_0|} \cdot \hat{i}\right), \qquad (12)$$

where $\hat{i}$ is the versor of the x axis. This was chosen to represent a crude approximation of a chemical bond. In this part we use three such potentials, which from now on we will label `harm1`, `harm10`, and `lj1`. The first two are defined by Eq. (11) with $k = 1$ and $k = 10\,\text{eV}/\text{Å}^2$, respectively. The third uses Eq. (12) with $\Delta V_r = 1\,\text{eV}, \mathbf{x}_0 = -2.5\hat{i}\,\text{Å}, r_0 = 1\,\text{Å}$, and $\Delta V_\alpha = 10\,\text{eV}$. It should be noted that the origin for the LJ potential was chosen because all simulations were run in box-shaped grids ranging from -2 to 2 Å. The grids had 200, 40, and 15 points of side, respectively, for 1D, 2D, and 3D. The wave function is considered zero outside of this space. Thus, this choice allows us to have the minimum of the potential inside the box without including the singularity, which could cause problems. The initial particle positions were generated in two different ways. The first method was to distribute the particles so that each grid element contains just the right amount to match the target distribution as closely as possible. The second instead employed a simple Monte Carlo method to randomly distribute them, following the target distribution but allowing for random fluctuations.

When calculating the energy within the MIW approximation in order to compare it to the energy found by diagonalizing the Hamiltonian, care needs to be taken. In the basic approach, forces are calculated on the hypothesis of perfectly pointlike particles, and they would in fact be exact for an infinite number of particles with infinitesimally small spacing. When using kernels, each particle contributes to the overall density with a distributed density. This can be interpreted as each particle representing, in fact, a large or infinite number of particles distributed according to that function and moving around

rigidly. This brings forth two main consequences for energy calculations:

(i) The ith particle's contribution to potential energy, V_i, should in theory not be calculated in a pointlike manner, $V(x_i)$, but rather as the integral

$$V_i = \int_{\mathbb{R}^D} V(\mathbf{x})\mathcal{K}(\mathbf{x})d\mathbf{x}. \qquad (13)$$

This might not always be possible in actual calculations. In that case, the pointlike approximation is accurate to first order, since the kernel is symmetric. If one has access to the second derivative of the potential, it is possible to expand it in Taylor series and find a third-order approximation, which also depends on b.

(ii) There is an "internal energy" correction for each particle, consisting of the many-world-interaction energy of the particles constituting the Gaussian distribution kernel itself. This is a constant term and can be calculated by applying Eq. (4), replacing the probability density in Eq. (5) with the kernel function and the sum over n with an integral over all space. Luckily, it is rather easy to calculate for both kernels:

$$U_{\text{corr}}^{(\text{Gauss})} = \frac{\hbar^2}{4m}\frac{D}{b^2}, \quad U_{\text{corr}}^{(\text{exp})} = \frac{\hbar^2}{8m}\frac{D}{b^2}. \qquad (14)$$

It should be remarked that this term is not required when comparing two MIW simulations with the same parameters, being constant; it becomes necessary, however, when considering simulations of different kinds or with different b.

The total energy is therefore computed as

$$E_{\text{tot}} = U_{\text{MW}}(\mathbf{X}) + U_{\text{corr}}^{(\text{kernel})} + \sum_i^N\left(V_i + \frac{1}{2}mv_i^2\right) \qquad (15)$$

though effectively the kinetic energy term at the end is zero for nondynamical calculations like this one and the search for the ground state presented in the next subsection. Figure 2 shows the error in energy calculated with the MIW approach for the various potentials and dimensionalities tested. A few observations are in order. Convergence is overall satisfactory in all cases, with various degrees of success. The 1D case shows obviously the advantages of the kernel approximation compared to the one given in Eq. (6). For the kernel approximation, both with Gaussian and exponential kernels, increasing the number of worlds used tends to reliably improve convergence, which eventually reaches a limit value. As a general rule, it seems that for these systems using any more than 50 worlds does not really bring any improvement in the approximation of the energy. The simpler method, on the other hand, converges only initially to then immediately diverge again when the density of worlds becomes too high, as its dependency on the inverse of the distance between world particles makes it far more sensitive to numerical errors. This is even more obvious for Monte Carlo generated particle configurations. This means that there is a nontrivial optimal amount of worlds to use, which in any real-world application would be another variable to consider when deciding the parameters for a calculation. In the 2D and 3D cases, random Monte Carlo initialization provides a better average approximation but also greater noise, whereas uniform distributions quickly converge to a slightly
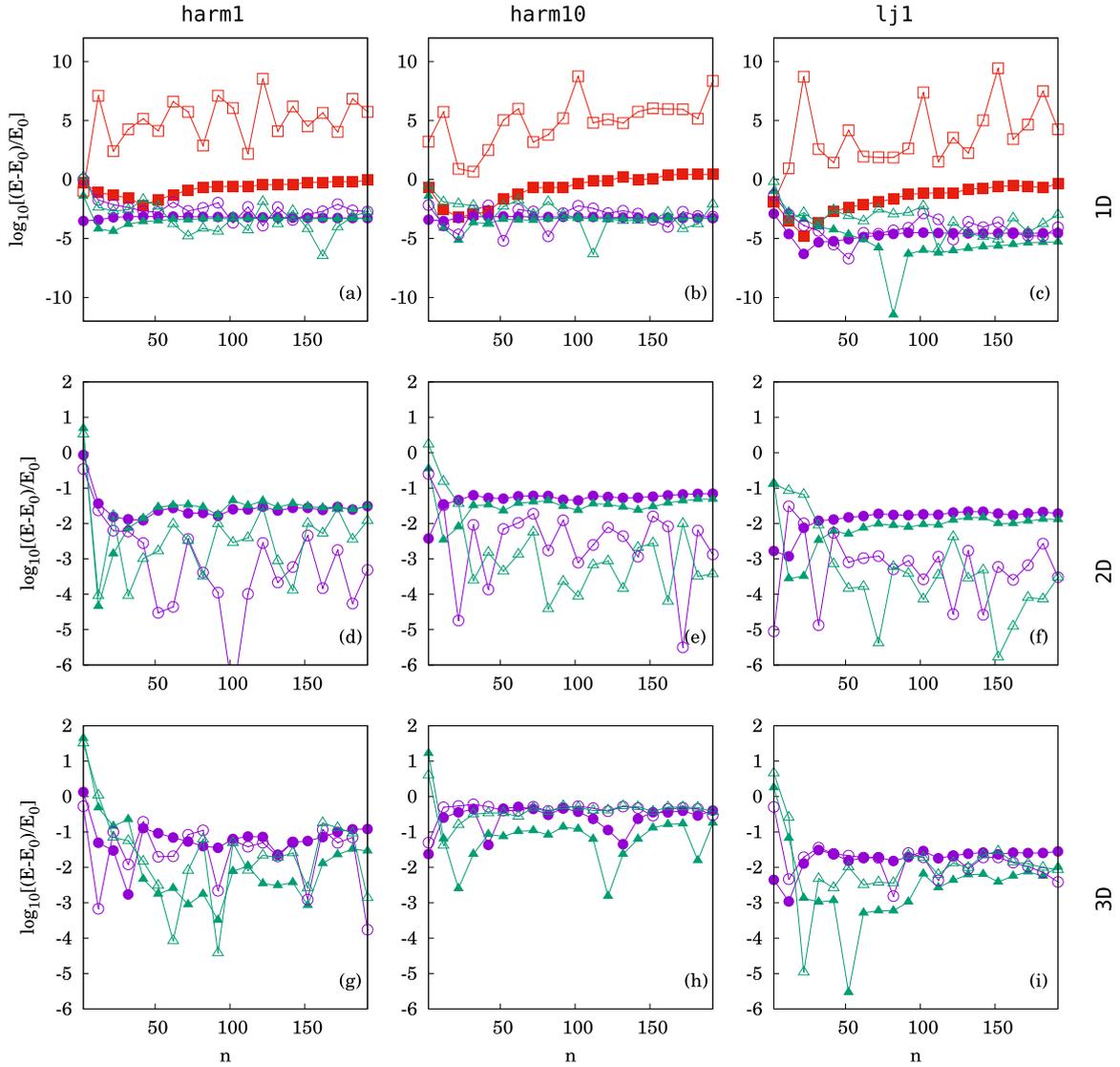
FIG. 2. Logarithmic plots of the MIW energy error with an ideal distribution vs number of worlds for various potentials and dimensionalities. Ideal energies were computed with a matrix Numerov algorithm using grids of 200, 40, and 15 points of side, respectively, for 1D, 2D, and 3D. Circles represent the Gaussian kernel, triangles the exponential one, and squares the method from the original paper (only applicable to 1D). Filled dots represent uniformly distributed particles, empty ones the Monte Carlo distributed ones. Legend: (a), (b), and (c) are 1D potentials; (d), (e), and (f) are 2D; (g), (h), and (i) are 3D. By potential type, (a), (d), and (g) use the `harm1` potential; (b), (e), and (h) use `harm10`; (c), (f), and (i) use `lj1`. The same labels apply to Figs. 3 and 4.

biased value. This is probably the effect of such distributions being dependent on the underlying grid, which introduces artefacts.

B. Ground-state convergence

Now we move on to investigating a method of finding the ground state of a potential by using the MIW approach. This is straightforward: we generate a system of a number of worlds (in all cases here, $N = 50$ was used) in some configuration that we consider a reasonable starting point, then we use some optimization routine to converge it down to a point where all forces are in equilibrium. Here we try two different approaches to this process. In addition to that, since it is possible that particles might get stuck in nonphysical configurations or

local minima, the simulation is periodically reinitialized by computing the density and using it to redistribute the particles. This was done using the uniform distribution method, which is found to give the better results. When a reinitialization is performed, the bandwidth is newly calculated, too, using the AMISE method. Here two methods were used. The first is a simple molecular-dynamics simulation, with a strong damping achieved by using a Langevin thermostat with $T = 0$ K and $\gamma = 10^{15}$ s^{-1}. For this simulation, 10 sequences of 1000 time steps with $dt_{\max} = 5 \times 10^{-17}$ s (3×10^{-17} s for the 3D case) were used, with one reinitialization between each sequence. The second uses the Scipy implementation of the BFGS optimization algorithm, using 10 sequences of a maximum of 40 iterations, with a tolerance of 1×10^{-5} eV/Å on the forces. The initial configuration was chosen to be a completely
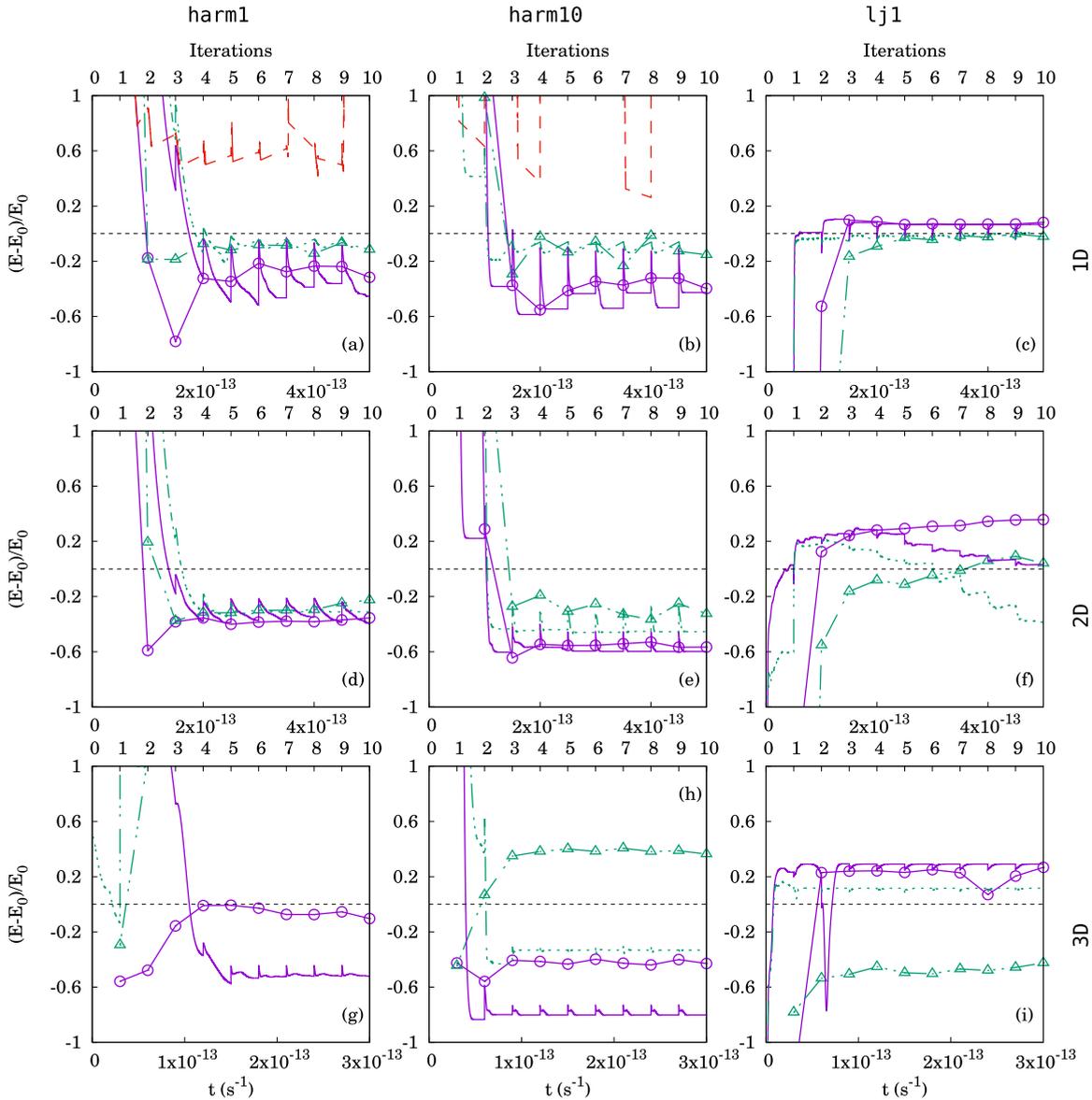
FIG. 3. Energy convergence during the relaxation process for different potentials and dimensionalities. Continuous lines represent the Gaussian kernel, dot-dashed lines the exponential one, and dashed lines the method from [13] converged with damped Langevin MD. Empty circles and triangles represent, respectively, the Gaussian and exponential kernels converged with the BFGS algorithm. For the labels, refer to the caption in Fig. 2.

uniform distribution for the harmonic potentials and a Gaussian centered on the minimum for the Lennard-Jones ones for the 1D and 2D cases. This choice was made because the latter, being much flatter on the long distance, risked causing convergence problems to an ensemble of particles that is too spread out. In the 3D case, a Gaussian of arbitrary width was used for all three potentials. This was not considered a problem as it seems reasonable to expect that in all practical applications similar assumptions could be made, and the classical minimum of the potential would likely be known from previous simulations.

The results of the calculation can be seen in Figs. 3 and 4 for convergence of energy over time and the root sum square (RSS) of the probability density error on the grid, which we label as χ. For energies obtained with the damped MD method, all points throughout all iterations are provided. For every other quantity,

only the final values of each of the 10 iterations is recorded instead. Energies and densities were compared to the known analytical solutions for harmonic potentials, and to numerically computed solutions for the Lennard-Jones one. For damped MD, the energy error clearly displays dents corresponding to each reinitialization, but after the first few iterations it generally falls back to its converged value. As a general rule, one can see the exponential kernel performing generally slightly better, except for the lj1 2D case, where the energy seems to diverge. For BFGS the behavior is often rather similar, with a few exceptions (for example, the energy and density of the 3D lj1 case with the exponential kernel have a bigger error than any other approach). In terms of performance, the damped MD method requires by definition 10 000 evaluations for both the energy and the forces of the entire system. By comparison, the BFGS runs required a number of energy and force evaluations
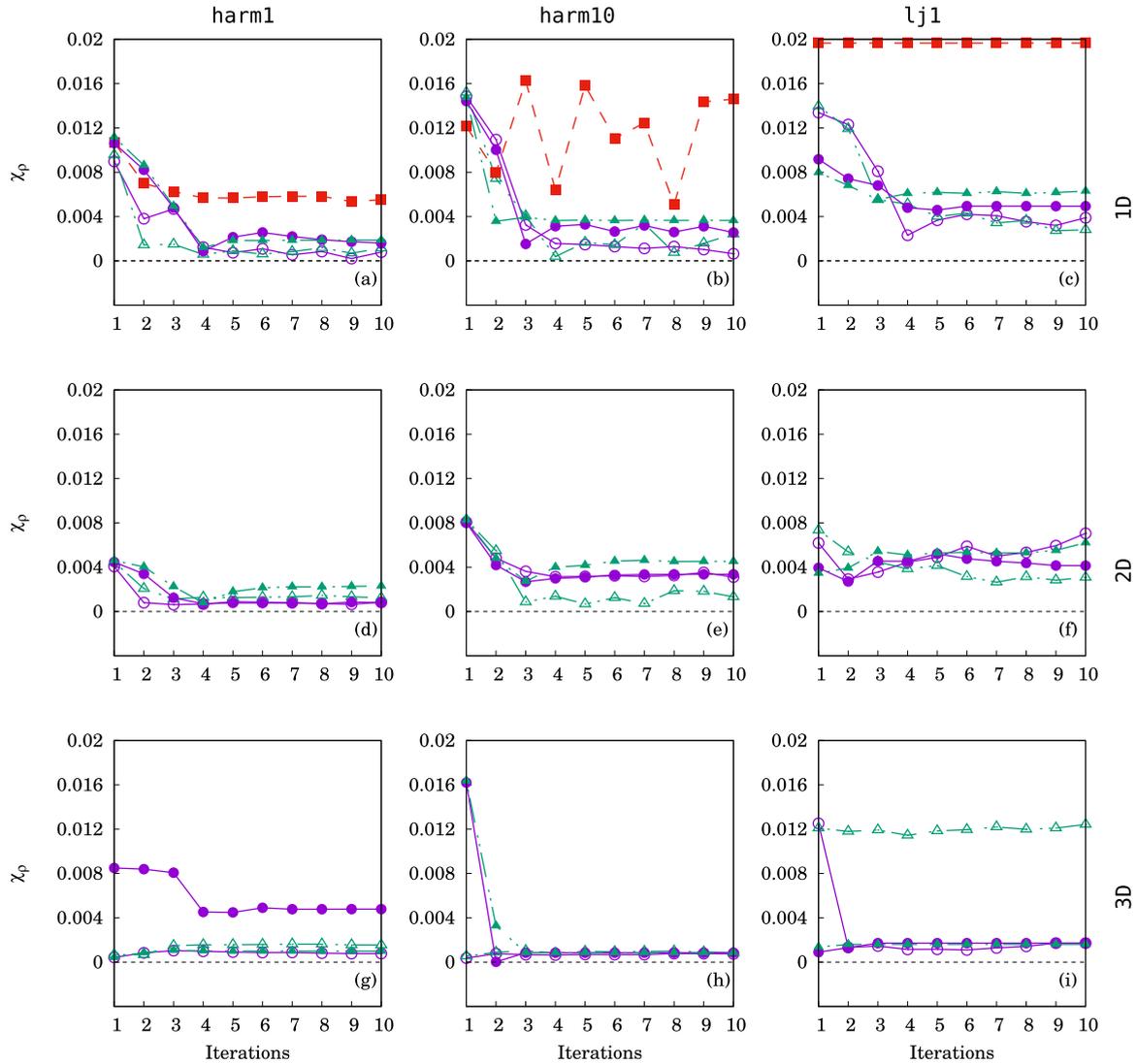
FIG. 4. Ground-state density error RSS convergence during the relaxation process for different potentials and dimensionalities. Circles represent the Gaussian kernel, and triangles represent the exponential one. Full markers represent damped MD, whereas empty ones represent BFGS. It was not possible to compute the quantity for the original method as it does not provide a continuous approximation for the density. For the labels, refer to the caption in Fig. 2.

both approximately comprised between 600 and 1800. From these results, one can see how the latter seems definitely much more computationally convenient, while producing results that are comparable to damped MD. This would be a unique advantage of this approach over the existing path-integral based techniques, which require a full MD run to produce results even for the ground state. In general, this approach to a ground-state search appears to be promising but potentially sensitive to the choices of parameters made. Periodically reinitializing the configuration or other corrective approaches can be used to prevent it from developing artefacts.

C. Finite-temperature effects

We now move on to examining a simple example of possible application of MIW simulations to the realm of finite-temperature quantum dynamics. While the original MIW theory does not explicitly mention temperature, there is no

reason to think that it should not be possible to simulate incoherent finite-temperature quantum dynamics by simply plugging one of the well-known MD thermostats into a MIW simulation. This is a consequence of the fact that thermostats approximate the system's interaction with the environment, and classical interactions between different particles in a MIW simulation are perfectly equivalent to the ones in a regular simulation. An interesting question is whether the thermostats should be correlated or coupled across worlds. Intuitively, correlated thermostats would represent an environment that is concentrated in a relatively small region of the phase space and evolves coherently in time, whereas uncorrelated thermostats would represent an environment widely dispersed in phase space and decohered. While there may be some interesting insights to be gained from exploring this matter, for the time being we will settle for fully uncorrelated thermostats, which seem to paint a much more realistic portrait of the situation, especially for high temperatures.
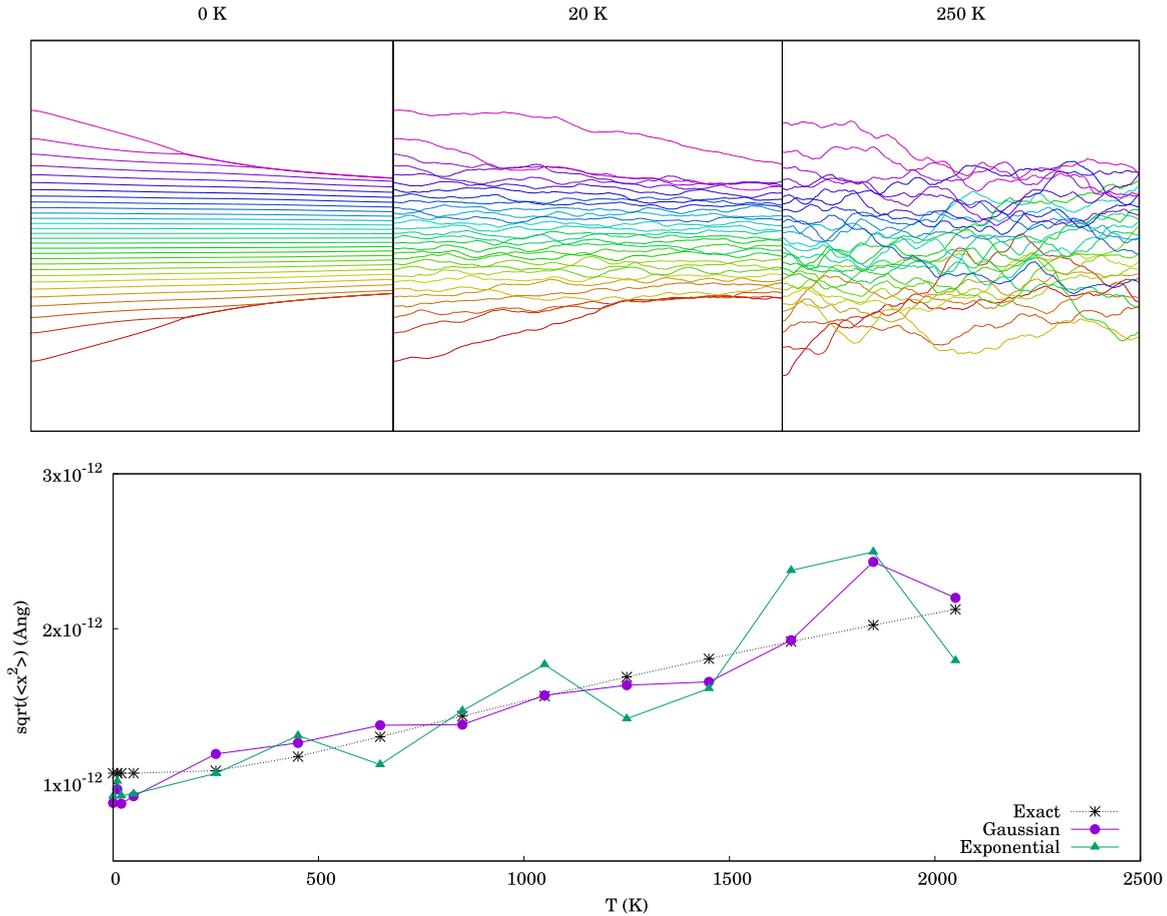
FIG. 5. Top: Many-interacting-world trajectories at different temperatures and computed value of $\sqrt{\langle x^2 \rangle}$ up to 2000 K for a particle in a harmonic oscillator with $k = 1$ eV/Å^2, using $N = 30$ MIW worlds and an exponential kernel. Bottom: standard deviation for theoretical and computed densities with Gaussian and exponential kernels as a function of temperature.

Figure 5 gives us a simple insight into how MIW simulations can reproduce thermal effects. The full bundle of trajectories, from the starting configuration to the end of a molecular-dynamics simulation, are shown for three different temperatures. The 0 K case is a perfect example of a damped MIW system converging to its ground state, with the contraction (driven by the external potential) being eventually countered by the repulsion due to the MIW potential, finding an equilibrium. It should be remarked, however, that while these are an approximation to "true" Bohmian trajectories, they are affected by the limits of the method. Specifically, at this temperature an artefact can be seen since at the fringes of the configuration the particles tend to "bunch up" instead of spreading more, as they should. This tends to happen even more when using a Gaussian kernel, which is affected by the problems described in Sec. II A. At the higher temperatures, the trajectories get scrambled and the system expands, which reduces the importance of this coalescence effect as well. The collisions may transfer further energy among particles so that fluctuations will be bigger than they would be in a noninteracting ensemble, and may allow particles to overcome barriers that should be impassable (thus allowing tunneling). Ultimately, when the temperature is high enough, the MIW potential's contribution becomes tiny compared to the thermostat forces, and the system reaches the classical limit.

The system chosen for testing whether the MIW approach can reproduce temperature-dependent quantum tunneling rates is a simple double well built by joining two harmonic potentials along a plane, as seen in Fig. 6. This system has been studied by Bell [28], and its tunneling rate temperature dependence is known. We choose a potential formed by two harmonic wells of $k = 10$ eV/Å^2 with $x_0 = 0.2$ Å. This leads to a potential barrier of $\Delta E = k x_0^2 / 2 = 0.2$ eV and turning points situated
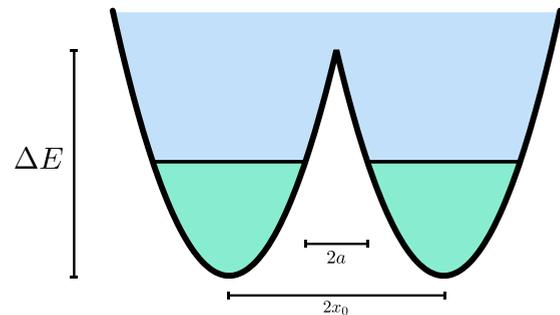

FIG. 6. Double harmonic well potential as described by Bell in [28]. The barrier height is ΔE, x_0 is the distance of the minimum from the barrier, and a is the distance of the turning point, namely the point where the potential exceeds the zero point energy of the particle.

at $a \sim 0.06$ Å. The Arrhenius classical jumping rate is

$$\nu_c = \nu_0 \exp\left(-\frac{\Delta E}{k_B T}\right),\qquad(16)$$

whereas the Bell quantum corrected version is

$$\nu_q = \nu_0 \frac{1}{\beta - \frac{\Delta E}{k_B T}}\left[\beta \exp\left(-\frac{\Delta E}{k_B T}\right) - \frac{\Delta E}{k_B T}\exp(-\beta)\right]\quad(17)$$

with

$$\beta = \frac{a\pi\sqrt{2m\Delta E}}{\hbar} \sim 1.77.\qquad(18)$$

Three separate simulations were run with $N = 50$ worlds: one with a Gaussian kernel, one with an exponential kernel, and one with no kernel forces at all, making it effectively 50 decoupled classical simulations. A Langevin thermostat with $\gamma = 10^{14}$ s^{-1} was used. Here a little digression is in order. It is common wisdom that Langevin thermostats should not be used when computing diffusion rates; however, there is reason to believe this is justified in this specific case. The rationale for not using it in ordinary MD simulations is that a Langevin thermostat fully couples each individual particle to the heat bath, and this is unrealistic for, e.g., molecules in a fluid. However, this is not the case here: we are effectively simulating only one particle, and each copy we do simulate is in fact fully coupled, classically, to its own heat bath, namely the rest of its world. There is no doubt, of course, that the chosen γ will control the time scale of the process (in fact, it seems hardly a coincidence that as seen later we will find $\nu_0 = \gamma$). However, since we are interested in comparing jumping rates, and how the MIW potential enhances them, rather than in their absolute values, this is not necessarily a problem. For multiparticle simulations of course the usual considerations would apply, and a Nosé-Hoover thermostat would be more suited to the task at hand. Tunneling was calculated by measuring the fraction of the density inside the starting well and fitting an exponential decay curve to it as it fell from its initial value of almost 1 (some leak-
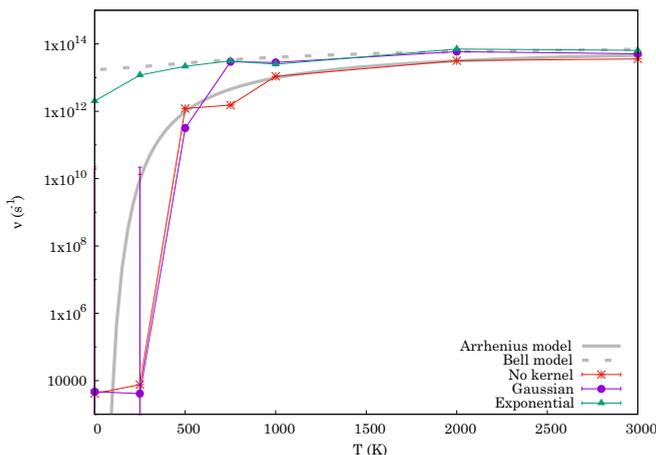

FIG. 7. Jumping rates in a MIW simulation on a double harmonic well potential. The fitted parameters are shown with error bars (though most of them are so small as to be invisible) and overlapped with the Arrhenius and Bell models.

age due to the tails of the distributions is present) to the equilibrium value of 0.5. The no-kernel simulation was used as a benchmark to fit the value of ν_0, using Eq. (16), which was then plugged into Eq. (17) to estimate the quantum jumping rate.

Figure 7 shows the final result. The Arrhenius model was fitted with $\nu_0 = 10^{14}$ s^{-1}, and the result applied to the Bell model. The rates originated from the exponential kernel simulations follow it closely, showing that the quantum MIW potential does indeed enhance the jumping process and reproduce the correct tunneling dynamics. The Gaussian kernel simulations behave closer to the ones without a kernel at the beginning and then catch up with the quantum model around $T = 750$ K. This is probably due to the already mentioned issue with particles "bonding" when using a smooth kernel, and the problem is overcome once the system has enough kinetic energy to break those pairs. The calculation suggests that it is indeed possible to simulate finite-temperature quantum-dynamical effects with the MIW method.

V. CONCLUSIONS AND FUTURE PROSPECTS

An extension to the many-interacting-worlds description of QM first introduced in [13] that makes use of kernel density estimation has been proposed. The method appears to give promising results in reproducing the solutions of simple quantum problems with an ensemble of coupled classical simulations, and it can pave the way to real-time finite-temperature quantum dynamics for *ab initio* molecular dynamics and the study of quantum nuclear effects. Some details of the method need to be better understood before applying it to molecular-dynamics problems. For example, the Gaussian kernel has been shown often to perform worse than the exponential one due to its smoothness; however, the same quality makes it ideal to approximate the true density distribution. A way to overcome the smoothness problem would be desirable. One possibility would be to make the kernel width b a dynamical variable, allowing kernels to squeeze when two particles come too close so that their repulsion grows and they never get to the point of overlapping. This would make the calculations more complex, but it would also add more degrees of freedom to the system and possibly make it better at approximating the true wave function. A recent work [29] also suggests a connection between the choice made for probability density reconstruction and which quantum state the particles effectively approximate. The logic is hard to translate to the kernel method used here, but if possible it might shed some light on a way to simulate excited states specifically. The work done in [20] shows how this can effectively work in 1D, provided that the positions of the nodes of the wave function are known beforehand. Finally, the analogies between the MIW and the PIMD methods are striking and suggest that a deeper connection between the two might exist. Studying that might bring new insights into how to mitigate each method's weaknesses by mixing it with the other.

APPENDIX A: CALCULATION OF QUANTUM FORCES WITH GAUSSIAN AND EXPONENTIAL KERNELS

We now show how Eq. (4) and its derivatives can be computed efficiently assuming the probability is constructed with a Gaussian kernel, as seen in (7). This formalism is designed to make for especially compact code when working with languages that allow for elementwise array operations such as FORTRAN or PYTHON+Numpy. Let us consider the case of a single quantum particle represented with N worlds in D dimensions. The coordinate of the particle in world i along dimension k is written as $x_i^{(k)}$. Let us also consider a kernel of fixed bandwidth b. Then we define

$$r_{ij}^{(k)} = x_i^{(k)} - x_j^{(k)}, \quad r_{ij}^2 = \sum_k \left(r_{ij}^{(k)}\right)^2,$$

$$P_{ij} = \frac{1}{N(\sqrt{\pi}b)^D} \exp\left(-\frac{r_{ij}^2}{b^2}\right), \tag{A1}$$

$$P_{ij}^{\prime(k)} = -\frac{2}{b^2} r_{ij}^{(k)} P_{ij}, \quad P_{ij}^{\prime\prime} = -\frac{2}{b^2}\left(1 - \frac{2}{b^2} r_{ij}^2\right) P_{ij}.$$

In this formalism, P_{ij} represents the contribution of particle j to the density probability at the position of particle i, P_{ij}' is its gradient with respect to the position of particle i, and so on. It should be noted that, while we included the normalization factor in Eq. (A1), this is not really relevant for the final forces as it disappears in the formulation of U_{MW}, which contains a ratio between the kernel and its derivative. Computing the total quantities, summed over all particles, requires a bit more care. If we define

$$P_i = \sum_j P_{ij} \tag{A2}$$

as the total density probability at the position of particle i, then its derivatives are

$$\frac{dP_i}{dx_n^{(l)}} = \begin{cases} P_n^{\prime(l)}, & n = i, \\ -P_{in}^{\prime(l)}, & n \neq i, \end{cases} \tag{A3}$$

and the second ones are

$$\frac{dP_i^{\prime(k)}}{dx_n^{(l)}} = \begin{cases} P_n^{\prime\prime(l)}, & n = i, l = k, \\ -P_{in}^{\prime\prime(l)}, & n \neq i, l = k, \\ -\frac{2}{b^2} \sum_j r_{nj}^{(k)} P_{nj}^{\prime(l)}, & n = i, l \neq k, \\ \frac{2}{b^2} r_{in}^{(k)} P_{in}^{\prime(l)}, & n \neq i, l \neq k, \end{cases} \tag{A4}$$

where the quantities with only one index (P_n', P_n'') represent sums over j as seen in Eq. (A2). Using these relationships, it is straightforward, if rather tedious, to compute the interworld potential and the forces. We can rewrite Eq. (4) for this kernel using the new formalism:

$$g_i^{(k)} = \frac{\hbar}{2} \frac{P_i^{\prime(k)}}{P_i}, \quad U = \frac{1}{2m} \sum_{i,k} \left[g_i^{(k)}\right]^2. \tag{A5}$$

Then the full derivative with respect to the particle positions can be written as

$$\frac{dU}{dx_n^{(l)}} = 2g_n^{(l)} \left[-\frac{1}{P_n^2}\left(P_n^{\prime(l)}\right)^2 + \frac{1}{P_n} P_n^{\prime\prime(l)} \right]$$

$$+ \sum_{i \neq n} 2g_i^{(l)} \left[\frac{1}{P_i^2} P_{in}^{\prime(l)} P_i^{\prime(l)} - \frac{1}{P_i} P_{in}^{\prime\prime(l)} \right]$$

$$+ \sum_{k \neq l} 2g_n^{(k)} \left[-\frac{1}{P_n^2} P_n^{\prime(k)} P_n^{\prime(l)} - \frac{2}{b^2 P_n} \sum_j r_{nj}^{(k)} P_{nj}^{\prime(l)} \right]$$

$$+ \sum_{i \neq n, k \neq l} 2g_i^{(k)} \left[\frac{1}{P_i^2} P_{in}^{\prime(k)} P_i^{\prime(l)} + \frac{2}{b^2 P_i} r_{in}^{(k)} P_{in}^{\prime(l)} \right], \tag{A6}$$

where it should be noted that the two bottom summation terms are always going to be zero in the one-dimensional case, which therefore noticeably simplifies the expression. The forces of course are going to be equal to this expression with a minus sign. Now we consider the case of an exponential kernel. A lot of the passages are similar, but we need to take into account the different form of the derivatives. In this case, we have

$$r_{ij} = \sqrt{\sum_k \left(r_{ij}^{(k)}\right)^2},$$

$$P_{ij} = \frac{\Gamma(D/2)}{2N(D-1)!(\sqrt{\pi}b)^D} \exp\left(-\frac{r_{ij}}{b}\right),$$

$$P_{ij}^{\prime(k)} = -\frac{1}{b} \frac{r_{ij}^{(k)}}{r_{ij}} P_{ij},$$

$$P_{ij}^{\prime\prime} = -\frac{1}{b} \frac{1}{r_{ij}} \left[1 - \frac{\left(r_{ij}^{(k)}\right)^2}{r_{ij}^2} - \frac{1}{b} \frac{\left(r_{ij}^{(k)}\right)^2}{r_{ij}} \right] P_{ij}. \tag{A7}$$

With these new assignments, Eq. (A3) still holds for first derivatives, whereas second derivatives become

$$\frac{dP_i^{\prime(k)}}{dx_n^{(l)}} = \begin{cases} P_n^{\prime\prime(l)}, & n = i, l = k, \\ -P_{in}^{\prime\prime(l)}, & n \neq i, l = k, \\ -\sum_j \frac{r_{nj}^{(k)}}{r_{nj}} \left(\frac{1}{r_{nj}} + \frac{1}{b}\right) P_{nj}^{\prime(l)}, & n = i, l \neq k, \\ \frac{r_{in}^{(k)}}{r_{in}} \left(\frac{1}{r_{in}} + \frac{1}{b}\right) P_{in}^{\prime(l)}, & n \neq i, l \neq k, \end{cases} \tag{A8}$$

and therefore the forces

$$\frac{dU}{dx_n^{(l)}}$$

$$= 2g_n^{(l)} \left[-\frac{1}{P_n^2}\left(P_n^{\prime(l)}\right)^2 + \frac{1}{P_n} P_n^{\prime\prime(l)} \right]$$

$$+ \sum_{i \neq n} 2g_i^{(l)} \left[\frac{1}{P_i^2} P_{in}^{\prime(l)} P_i^{\prime(l)} - \frac{1}{P_i} P_{in}^{\prime\prime(l)} \right]$$

$$+ \sum_{k \neq l} 2g_n^{(k)} \left[-\frac{1}{P_n^2} P_n^{\prime(k)} P_n^{\prime(l)} \right]$$

$$-\frac{1}{P_n}\sum_j \frac{r_{nj}^{(k)}}{r_{nj}}\left(\frac{1}{r_{nj}}+\frac{1}{b}\right)P_{nj}'^{(l)}\Bigg]$$

$$+\sum_{i\neq n,k\neq l} 2g_i^{(k)}\left[\frac{1}{P_i^2}P_{in}'^{(k)}P_i'^{(l)}+\frac{1}{P_i}\frac{r_{in}^{(k)}}{r_{in}}\left(\frac{1}{r_{in}}+\frac{1}{b}\right)P_{in}'^{(l)}\right].$$

$$\tag{A9}$$

APPENDIX B: NORMALIZATION OF THE EXPONENTIAL KERNEL

The multivariate exponential kernel centered in the origin is defined as

$$\mathcal{K}(\mathbf{q})=\exp\left[-\frac{|\mathbf{q}|}{b}\right] \tag{B1}$$

for a given width b. This needs to be divided by its integral over the entire space for normalization purposes. For the 1D case the solution is simple, as the integral

$$\int_0^\infty \exp\left(-\frac{x}{b}\right)dx = b \tag{B2}$$

is easily found, and thus the overall integral is $2b$. However, the multivariate case is more complex. One can find it considering two things. First, the integral of a radial function in a D-dimensional space can be defined as

$$\int_{\mathbb{R}^n} f(|\mathbf{q}|)d\mathbf{q}=\int_0^\infty f(r)\omega_{D-1}(r)dr, \tag{B3}$$

where ω_{D-1} is the surface area of the D-dimensional sphere [30]. This is known to be

$$\omega_{D-1}(r)=\frac{2\pi^{\frac{D}{2}}}{\Gamma\left(\frac{D}{2}\right)}r^{D-1}. \tag{B4}$$

On the other hand, the radial integral can be carried out by parts if we notice that

$$\int_0^\infty \exp\left(-\frac{r}{b}\right)r^{D-1}dr = \left|-b\exp\left(-\frac{r}{b}\right)r^{D-1}\right|_0^\infty \tag{B5}$$

$$+(D-1)b\int_0^\infty \exp\left(-\frac{r}{b}\right)r^{D-2}dr \tag{B6}$$

$$=(D-1)b\int_0^\infty \exp\left(-\frac{r}{b}\right)r^{D-2}dr \tag{B7}$$

as the first term goes to zero both on $r=0$ and $r=\infty$. We can repeat the operation $D-1$ times, thus finding

$$\int_0^\infty \exp\left(-\frac{r}{b}\right)r^{D-1}dr = (D-1)!b^D, \tag{B8}$$

which, combined with the prefactor for the surface area of an n-sphere, gives us

$$\int_{\mathbb{R}^D} \mathcal{K}(\mathbf{q})=\frac{2(\sqrt{\pi}b)^D}{\Gamma\left(\frac{D}{2}\right)}(D-1)!, \tag{B9}$$

whose reciprocal is the normalization factor we need.

APPENDIX C: A MATRIX NUMEROV METHOD FOR INTEGRATION OF THE SCHRÖDINGER EQUATION IN ARBITRARY DIMENSIONS

The original 1D matrix Numerov method for integrating the Schrödinger equation was presented in [26]. An analog scheme for the 2D equation is described in [31]. Here we write the same scheme in a general form for any number of dimensions. Similarly to what happens in 1D, the Numerov method is designed to solve equations of the form

$$\nabla^2\psi(\mathbf{x})=f(\mathbf{x})\psi(\mathbf{x}), \tag{C1}$$

where, in the case of the Schrödinger equation,

$$f(\mathbf{x})=-\frac{2m}{\hbar^2}[E-V(\mathbf{x})]. \tag{C2}$$

Now we expand ψ in a Taylor series, define the function on a grid, and consider the "stencil" surrounding a grid point composed of all nearest neighbors—the points that are one step forward or backward in each direction. Then we can write

$$\sum_i^D \frac{\psi(\mathbf{x}+h_i\boldsymbol{\epsilon}_i)-2\psi(\mathbf{x})+\psi(\mathbf{x}-h_i\boldsymbol{\epsilon}_i)}{h_i^2}$$

$$=f\psi+\frac{1}{12}\sum_i^D \frac{\partial^4\psi}{\partial x_i^4}h_i^2+O(h^6) \tag{C3}$$

with $\boldsymbol{\epsilon}_i$ a unit vector and h_i a grid step for dimension i. In this case, the following relation holds:

$$\nabla^2(f\psi)=\nabla^2(\nabla^2\psi)=\sum_i^D \frac{\partial^4\psi}{\partial x_i^4}+\sum_i^D\sum_{j\neq i}^D \frac{\partial^4\psi}{\partial x_i^2\partial x_j^2} \tag{C4}$$

so we can separate

$$\sum_i^D \frac{\psi(\mathbf{x}+h_i\boldsymbol{\epsilon}_i)-2\psi(\mathbf{x})+\psi(\mathbf{x}-h_i\boldsymbol{\epsilon}_i)}{h_i^2}$$

$$=f\psi+\frac{1}{12}\sum_i^D \frac{\partial^2(f\psi)}{\partial x_i^2}h_i^2-\frac{1}{12}\sum_i^D h_i^2\sum_{j\neq i}^D \frac{\partial^4\psi}{\partial x_i^2\partial x_j^2}. \tag{C5}$$

Now, considering that we are working within a grid of finite size, we can write all operators as matrices. The matrix $\mathbf{A}$ as described in [26] extends to a Kronecker sum:

$$\mathbf{A}^{(D)}=\sum_i^D \mathbf{A}_i^{(D)}=\bigoplus_i^D \frac{(\mathbb{I}_{-1}-2\mathbb{I}_0+\mathbb{I}_1)}{h_i^2} \tag{C6}$$

while the matrix $\mathbf{B}$, which operates on $f\psi$ on the right-hand side, becomes

$$\mathbf{B}^{(D)}=\mathbb{I}+\frac{1}{12}\sum_i^D h_i^2\mathbf{A}_i^{(D)}. \tag{C7}$$

We can also write the mixed derivatives as matrix products,

$$\frac{\partial^4}{\partial x_i^2\partial x_j^2}\rightarrow \mathbf{A}_i^{(D)}\mathbf{A}_j^{(D)}, \tag{C8}$$

which happen to commute since the $\mathbf{A}$ matrices are symmetric. So in the end we can write the multidimensional equivalent of

the 1D Numerov method as

$$-\frac{\hbar^2}{2m}\left[\mathbf{A}^{(D)} + \frac{1}{12}\sum_{i,j>i}\mathbf{A}_i^{(D)}\mathbf{A}_j^{(D)}\left(h_i^2 + h_j^2\right)\right]\psi$$

$$= \mathbf{B}^{(D)}(E - \mathbf{V})\psi$$

$$\Rightarrow -\frac{\hbar^2}{2m}\mathbf{B}^{-1(D)}\left[\mathbf{A}^{(D)} + \frac{1}{12}\sum_{i,j>i}\mathbf{A}_i^{(D)}\mathbf{A}_j^{(D)}\left(h_i^2 + h_j^2\right)\right]$$

$$\times\, \psi + \mathbf{V}\psi = E\psi \tag{C9}$$

with $\mathbf{V}$ a matrix having the potential along its diagonal and zero everywhere else. Therefore, this becomes an eigenvalue problem that can be solved by diagonalizing the matrix:

$$\mathbf{M} = -\frac{\hbar^2}{2m}\mathbf{B}^{-1(D)}\left[\mathbf{A}^{(D)} + \frac{1}{12}\sum_{i,j>i}\mathbf{A}_i^{(D)}\mathbf{A}_j^{(D)}\left(h_i^2 + h_j^2\right)\right] + \mathbf{V} \tag{C10}$$

and will give us energies and eigenstates as a result.

[1] R. Car and M. Parrinello, Phys. Rev. Lett. **55**, 2471 (1985).

[2] M. Born and R. Oppenheimer, Ann. Phys. **389**, 457 (1927).

[3] X.-Z. Li, M. I. J. Probert, A. Alavi, and A. Michaelides, Phys. Rev. Lett. **104**, 066102 (2010).

[4] B. Pamuk, J. M. Soler, R. Ramírez, C. P. Herrero, P. W. Stephens, P. B. Allen, and M.-V. Fernández-Serra, Phys. Rev. Lett. **108**, 193003 (2012).

[5] K. T. Wikfeldt, J. Phys.: Conf. Ser. **571**, 012012 (2014).

[6] Z. D. Nagel and J. P. Klinman, Chem. Rev. **106**, 3095 (2006).

[7] D. Marx and M. Parrinello, Z. Phys. B: Condens. Matter **95**, 143 (1994).

[8] A. Witt, S. D. Ivanov, M. Shiga, H. Forbert, and D. Marx, J. Chem. Phys. **130**, 194510 (2009).

[9] J. Cao and G. A. Voth, J. Chem. Phys. **99**, 10070 (1993).

[10] S. Habershon, D. E. Manolopoulos, T. E. Markland, and T. F. Miller III, Annu. Rev. Phys. Chem. **64**, 387 (2013).

[11] X.-Z. Li, B. Walker, and A. Michaelides, Proc. Natl. Acad. Sci. USA **108**, 6369 (2011).

[12] Y. V. Suleimanov, R. Collepardo-Guevara, and D. E. Manolopoulos, J. Chem. Phys. **134**, 044131 (2011).

[13] M. J. W. Hall, D.-A. Deckert, and H. M. Wiseman, Phys. Rev. X **4**, 041013 (2014).

[14] P. Holland, Ann. Phys. **315**, 505 (2005).

[15] J. Schiff and B. Poirier, J. Chem. Phys. **136**, 031102 (2012).

[16] D. Bohm, Phys. Rev. **85**, 166 (1952).

[17] D. Bohm, Phys. Rev. **85**, 180 (1952).

[18] M. Rosenblatt, Ann. Math. Statist. **27**, 832 (1956).

[19] E. Parzen, Ann. Math. Statist. **33**, 1065 (1962).

[20] H. Herrmann, M. J. W. Hall, H. M. Wiseman, and D.-A. Deckert, arXiv:1712.01918.

[21] I. Poltavsky and A. Tkatchenko, Chem. Sci. **7**, 1368 (2016).

[22] R. Fletcher, *Practical Methods of Optimization* (Wiley, Chichester, 1987).

[23] I. R. Craig and D. E. Manolopoulos, J. Chem. Phys. **121**, 3368 (2004).

[24] S. van der Walt, S. C. Colbert, and G. Varoquaux, Comput. Sci. Eng. **13**, 22 (2011).

[25] E. Jones, T. Oliphant, P. Peterson *et al.*, SciPy: Open source scientific tools for Python (2001), http://www.scipy.org/.

[26] M. Pillai, J. Goglio, and T. G. Walker, Am. J. Phys. **80**, 1017 (2012).

[27] S. J. Sheather, Statist. Sci. **19**, 588 (2004).

[28] R. P. Bell, *The Tunnel Effect in Chemistry* (Chapman and Hall, New York/London, 1980).

[29] I. W. McKeague, E. A. Peköz, and Y. Swan, arXiv:1606.06618.

[30] K. R. Stromberg and A. M. Society, *An Introduction to Classical Real Analysis* (Wadsworth International Group, Belmont, CA, 1981).

[31] A. Mohebbi and M. Dehghan, J. Computat. Appl. Math. **225**, 124 (2009).